Plant Soil (2026) 526:891–907
https://doi.org/10.1007/s11104-026-08983-w

RESEARCH ARTICLE

Root oxygen governs dryland ecosystem stability

Dongliang Han · Lei Ding · Guolong Zhang · Jianping Huang · Li Fu · Ming Peng · Changyu Li · Xiaoyue Liu

Received: 9 May 2026 / Accepted: 8 August 2026 / Published online: 21 August 2026
© The Author(s) 2026

Abstract

Background and Aims Roots are essential components of soil organisms and play pivotal roles in sustaining ecosystem stability. As drylands support over 38% of the global population and face unprecedented stability risks under anthropogenic warming, identifying the drivers of their stability is critical for early interventions to safeguard global food security. Divergent from the conventional view that higher soil biodiversity consistently enhances ecosystem stability—wherein ecosystem stability is typically linked to temporal scales, various properties, organizational structures and multiple thresholds—we present a new insight: root tissue oxygen elemental content (Root-O) indicates and drives dryland ecosystem stability.

Methods We integrated multiple approaches: satellite datasets (including global air temperature, soil biodiversity index, among others), field surveys (encompassing plant, soil, root and litter samples from multiple study sites in 2022), laboratory analyses (comprising elemental analyses of carbon, hydrogen, oxygen, and nitrogen across different sample properties), and global model simulations from the Sixth Coupled Model Intercomparison Project (CMIP6) were used to assess sensitive indicators driving threshold variations during 1950–2100.

Results We find that Root-O explains more variation in dryland ecosystem stability than plant, litter, and soil properties. Under different Shared Socioeconomic Pathways (SSPs) scenarios, CMIP6 projections indicate that the dynamics of sensitive indicators driving threshold variations in relation to ecosystem stability will likely be governed by the pronounced Root-O by the end of 2100.

Conclusions The dependence of dryland ecosystem stability on Root-O dynamic mechanisms should be considered in "FeiTian" Ecological Security Grand Model to accurately predict ecological risk under changing environments.

Keywords Oxygen and carbon cycles · Ecological stoichiometry · Ecosystem services · Dryland sustainability · Climate change

Responsible Editor: Ji Chen.

D. Han · L. Ding · G. Zhang · J. Huang (✉) · L. Fu · M. Peng · C. Li · X. Liu
Collaborative Innovation Center for Western Ecological Safety, Lanzhou University, Lanzhou, China
e-mail: hjp@lzu.edu.cn

D. Han · L. Ding · G. Zhang · J. Huang · L. Fu · M. Peng · C. Li · X. Liu
College of Atmospheric Sciences, Lanzhou University, Lanzhou, China

Introduction

Under a 2.0 ℃ global warmingscenario in the twenty-first century, drylands (defined as regions with total annual precipitation/potential evapotranspiration < 0.65) are projected to warm by 3.2℃–4.0

℃—approximately 44% more than the 2.4℃–2.6 ℃ increase expected for humid regions (Huang et al. 2017). Traditionally, soil biodiversity has been recognized as a critical determinant of dryland ecosystem stability under climate warming (Qi et al. 2026). That is, higher soil biodiversity strengthens ecosystem stability, while lower biodiversity diminishes it (Qi et al. 2026). This is because, variations in soil biodiversity modulate vegetation cover (e.g. by enhancing nutrient uptake) and litter accumulation (e.g. by promoting leaf growth and subsequent senescence and abscission), which are closely linked to soil organic carbon storage and soil water content—the key powerhouse and regulator of ecosystem processes (Fu et al. 2025). Such responses cascade through dryland ecosystems, exerting profound impacts on ecosystem stability and multifunctionality (Berdugo et al. 2020; Fu et al. 2025; Han et al. 2025). Therefore, ecosystem stability is usually defined as the time-averaged productivity of plants divided by the standard deviation of this productivity (Yang et al. 2018). Based on this conventional definition, in this work, we first decomposed ecosystem stability into four dimensions characterized by plant, litter, soil and root components: temporal scales, various properties, organizational structures, and multiple thresholds. Second, we identified sensitive indicators regulating ecosystem changes within the multiple-threshold framework. Third, we explored the key factors governing these indicators, which were defined as the drivers of ecosystem stability (Fig.1).

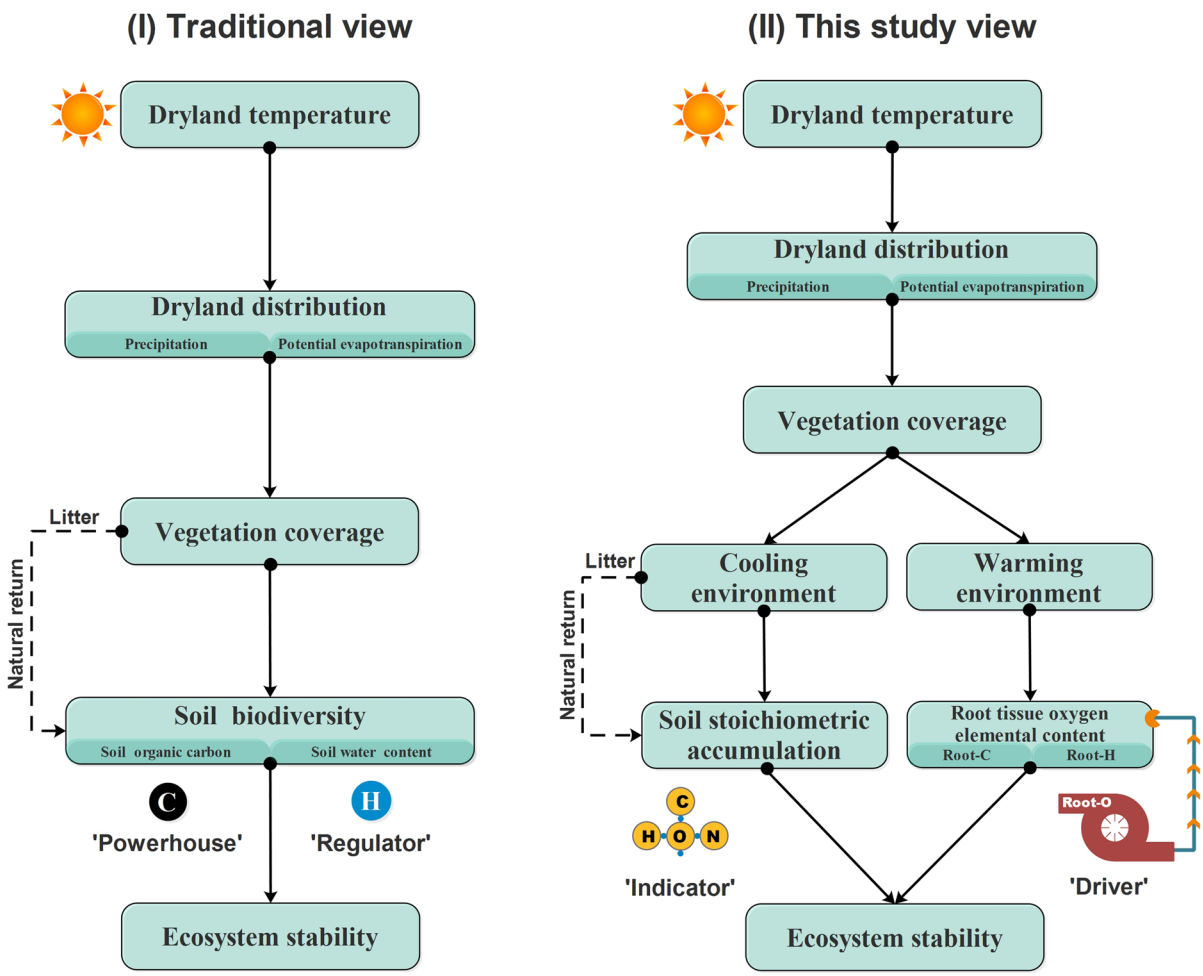


Fig. 1 Traditional and this study views of the nature of ecosystem stability affect how we predict and manage key properties

Root tissue oxygen elemental content (denoted as Root-O), loosely analogous to blood oxygen saturation in the human body—declining during strenuous exercise—plays a pivotal role in climate modulation, soil fertility maintenance, and crop yield maintenance (Ascha et al. 2018; Greabu et al. 2008; Huang et al. 2020a; Toro et al. 2018). It is also central to vegetation's water uptake and a dominant controller of nutrient cycling, governing the storage of carbon and nitrogen within soil (Greabu et al. 2008; Ridgeway et al. 2024). Vegetation absorbs CO_2 through photosynthesis and emits O_2, while respiration consumes O_2 and releases CO_2 (Calvin 1956). The content of a given element in plant tissues reflects its uptake and accumulation patterns (Liu et al. 2024). For instance, Root-O is closely linked to oxygen absorption and utilization by root systems and exerts a vital driving effect on the accumulation and partitioning of root tissue carbon content (Root-C) (Toro et al. 2018). Such carbon–oxygen coupled dynamics regulate atmospheric composition, energy flow, and ecosystem stability (Berdugo et al. 2020; Huang et al. 2020a). Understanding how carbon and oxygen cycles interact and respond to climate change is therefore critical for predicting ecosystem functions and global biogeochemical feedbacks (Han et al. 2022; Li et al. 2021).

How to systematically and effectively quantify the dynamic processes of Root-O and its related elements across dryland ecosystems. Ecological stoichiometry represents an approach in which elements serve as a common currency to analyze the scaling of trophic dynamics across four dimensions: temporal scales, various properties, organizational structures, and multiple thresholds within a plant-litter-soil-root system (Liu et al. 2025; Luo et al. 2025; Sterner and Elser 2002). This approach also facilitates quantitative analyses of biogeochemical cycles across dryland ecosystems and lays the theoretical foundation for the ecological stoichiometry paradigm (Grünzweig et al. 2022). For instance, when the soil C:N ratio approaches the optimal range for microbial growth (approximately 10–15:1), microbial decomposition of organic matter reaches its highest efficiency, allowing for the continuous release of plant-available inorganic nitrogen and maintaining the smooth operation of nutrient cycling (Kuzyakov and Xu 2013). Indeed, multiple thresholds modulated by plant-litter-soil-root elemental composition are central to the stoichiometric homeostasis concept that forms the basis of the ecological stoichiometry framework, within which we identified sensitive indicators controlling ecosystem dynamics (Persson et al. 2010). Meanwhile, ecosystem sensitivity indicators can be constrained by a range of outer cycling mechanisms (e.g. external exchange) and inner cycling mechanisms (e.g. self-selection), which together act to sustain the stability of local ecosystems (Chameides and Perdue 1997).

Ecosystem stability is a widely studied scientific theme attracting researchers from geography, meteorology and many other fields, and growing numbers of scholars within the emerging interdisciplinary artificial intelligence domain have begun to conduct matching exploratory analyses (Li and Guo 2025). For instance, the launch of the "Fundamental and Interdisciplinary Disciplines Breakthrough Plan of the Ministry of Education of China" in 2025 presents a pivotal opportunity to utilize artificial intelligence technology construct a "FeiTian" Ecological Security Grand Model. One of the goals of this model, which is grounded in multi-sphere interactions, is to predict the key drivers of ecosystem stability. Although the present study does not involve the "FeiTian" Ecological Security Grand Model, this work proposes a prospective research avenue for subsequent investigations in the future: integrating Root-O into the "FeiTian" Ecological Security Grand Model may advance predictive performance regarding the stability of fragile and sensitive ecosystems.

This study first quantifies the relative importance of traditionally focused indicators—including soil biodiversity index, air temperature, aridity index, leaf area index, soil organic carbon stock, and soil water content—in regulating the ecosystem stability across global drylands. Following the analytical framework proposed by (Chen et al. 2019), we further adopt three statistical analyses, namely partial correlation analysis, variation partitioning assessment, and structural equation modelling, to disentangle the relative contributions of driving factors to the variations in ecosystem sensitivity indicators. These analyses are ground in*in-situ* observations of ecological stoichiometry characteristics of in plants, litter, soil and roots along a cooling-to-warming temperature gradient. Building on the above analytical outcomes, we explore future changes in core sensitivity metrics associated with dryland ecosystem stability under multiple Shared Socioeconomic Pathways (SSPs) within the framework of the Couple Model Intercomparison Project

Phase 6 (CMIP6). Therefore, the objectives of this study were to: (1) identify key factors that act as both indicators and drivers governing dryland ecosystem stability across diverse temporal scales, various properties, organizational structures, and multiple thresholds; and (2) establish a framework model to assess dryland ecosystem stability and characterize future demand for Root-O supply across different global dryland regions.

Materials and methods

Global shifts in key factors underpinning dryland ecosystem stability

Based on the aridity index (AI, total annual precipitation/potential evapotranspiration) values, drylands can be further classified as semi-arid ($0.20 \leq AI < 0.50$), dry sub-humid ($0.50 \leq AI < 0.65$), arid ($0.05 \leq AI < 0.20$) as well as extremely arid ($AI < 0.05$) areas (Huang et al. 2016; Hulme 1996). The AI is provided by (Guan and Huang 2024) and calculated from 1961–1990, and the spatial resolution of the data is 0.5° by 0.5°. In addition, five other types of datasets related to the stability of global dryland ecosystems were used in this study. One is the global dataset of mean surface air temperature anomaly (ΔT), where ΔT for each pixel in a given year is defined as the value for the 2015_2000 period minus that for the 1981_2010 baseline period (Huang et al. 2020b). The second dataset stands for the satellite-observed leaf area index (LAI) product (global inventory monitoring and mapping system, GIMMS-LAI3g), which was used to analyze vegetation dynamics over the period from 1983 to 2014 (Zhang et al. 2023). The third dataset denotes the 2016 global soil biodiversity index, which ranges from 'organic materials' to 'solid rock' and is available athttps://esdac.jrc.ec.europa.eu/content/global-soil-biodiversity-atlas(Fu et al. 2025). The fourth dataset corresponds to the global soil organic carbon stock, which covers a soil depth of 0–30 cm and is of data version 1.2, with the data collection period spanning 2016–2017 (Zhang et al. 2023). The fifth dataset represents the mean annual soil water content across drylands, characterized by a soil depth of ~ 30 cm and covering the period from 2000 to 2024 (Huang et al. 2020b) (Fig.2).

In-situ observation data

The semi-arid grassland regions, accounting for 44.46%, play a significant role in the global annual-mean temperature trend of the land-surface, and meanwhile serve as critical ecological security barriers against the migration and expansion of desertification in arid zones (Huang et al. 2012). Therefore, we conduct long-term observational research on the stability of dryland ecosystems at the Semi-Arid Climate and Environment Observatory of Lanzhou University (SACOL, 1956.8 m above sea level, 35.946°N, 104.133°E). To acquire valuable observational data, SACOL serves as an optimal platform for investigating the drivers of ecosystem stability in climate—sensitive regions (Zhang et al. 2024). Specifically, the climate feature can be classified as the typical temperate semi-arid climate. The annual mean precipitation stands at 382 mm, while the mean evaporation reaches 1343 mm. The annual average air temperature is 6.7 ℃ and a relative humidity of 63% (Zhang et al. 2024). The underlying surface is predominantly occupied by short grass with species of*Tripolium vulgare*, *Artemisia frigida*, *Stipa bungeana*, and *Leymus secalinu*(Wang et al. 2010). The warming environment from May to October corresponds to a period of elevated temperatures that boost plant growth, the average temperature is 19 ℃ in July, yielding approximately 80% vegetation coverage and an average plant height of 15 cm, whereas the cooling environment spanning November to the following April features lower temperatures that inhibit vegetation growth and reduce the average plant height to roughly 10 cm, and the average temperature is−8℃ in January (Wang et al. 2010; Zhang et al. 2024). The parent soil material is primarily consisting of Quaternary aeolian loess, and in accordance with the World Reference Base for Soil Resources, the main soil type is sierozem (Wang et al. 2010).

In 2022, the climate conditions during our sampling period were found to be representative of the long-term average conditions for the region. Specifically, we compared key environmental parameters between 2017 and our sampling year (2022) from cooling (December) to warming (July) environments. These parameters included soil temperature and moisture at multiple depths (spanning 0–50 cm and 0–80 cm, respectively), as well as all components of the surface radiation budget (upward/downward

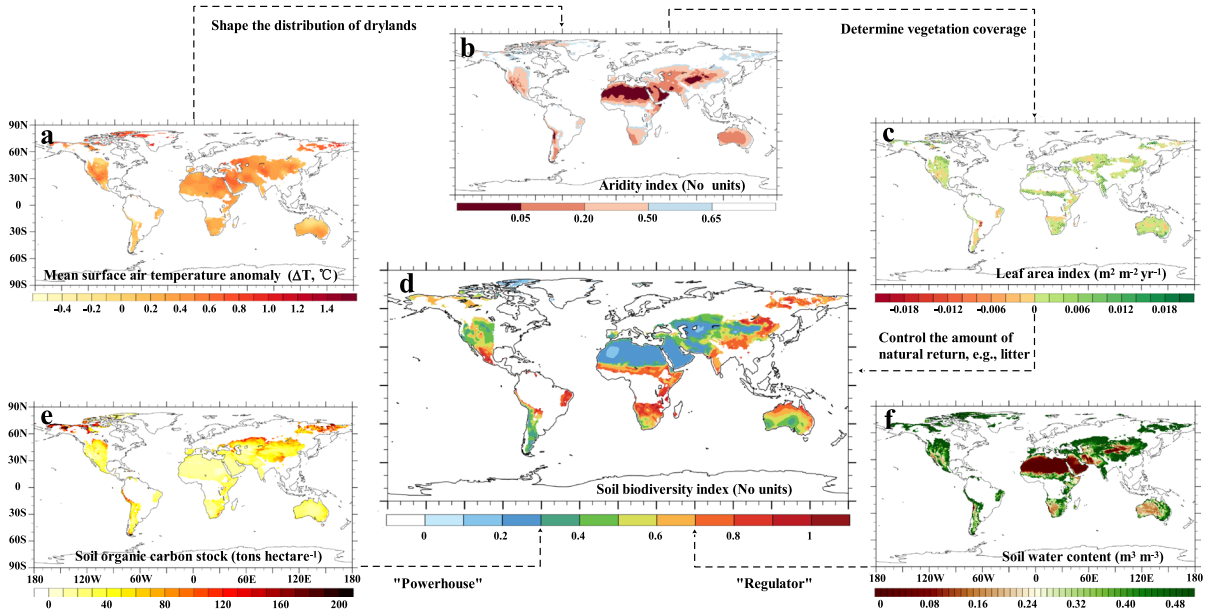


Fig. 2 Global distribution of key factors, their characteristics, or changes has exhibited distinct patterns in drylands over the past few decades. **a**, mean surface air temperature anomaly in all drylands [ΔT = (2015_2000)—(1981_2010), ℃]. **b**, the distribution of drylands based on aridity index (AI = the ratio of total annual precipitation to potential evapotranspiration, the mean AI from 1961 to 1990 climatology, unitless). **c**, the change of leaf area index during 1983–2014 over the dryland's regions, m^2 m^{-2} yr^{-1}; the stippling pattern denotes the 95% confidence level, as determined by a two-tailed Student's t-test. **d**, the soil biodiversity index of global drylands from 'organic materials' to 'solid rock' in 2016, unitless; the 'more is better' principle was characterized by a rise in the index. **e**, soil organic carbon stock in drylands, 0–30 cm soil depth, data version 1.2, 2016–2017, tons $hectare^{-1}$. **f**, mean annual soil water content over drylands, soil depth of 28 cm, 2000–2024, m^3 $m.^{-3}$

shortwave and longwave radiation). Statistical analysis confirmed the consistency of these environmental parameters across the five-year interval (refer to the Supplementary Information of (Zhu et al. 2024) for details). This demonstrates that the experimental period was characterized by stable climatic conditions, thereby minimizing the confounding influence of extreme weather and allowing for a robust interpretation of soil and plant nutrient dynamics. Field sampling followed the standardized technique described by (Maestre et al. 2022). Specifically, five 1.0 m × 1.0 m quadrats were established at 10 m intervals along a random transect in a flat, semi-arid grassland. Sampling occurred across multiple months (January, February, April, May, June, August, September, and November), spanning the seasonal transition from cool to warm conditions. All samples were collected in the middle of each month between 08:00 and 12:00 local time (Jiang et al. 2026).

Litter was first collected from each quadrat using a grass rake and placed into paper envelopes, after which all aboveground plant was harvested at ground level using scissors and stored separately. Subsequently, soil samples from the top 20 cm were collected at three diagonal points within each 1.0 m × 1.0 m quadrat using a 5-cm diameter soil corer and then pooled to form a single composite sample; similarly, root samples were extracted at adjacent locations to a depth of 20 cm using an 8-cm diameter root corer and homogenized into one sample per quadrat. Soil and root samples were transported to the laboratory. Soil samples were air-dried, and visible roots and stones were removed. Root samples were rinsed with tap water to remove soil particles. For biomass determination, plant, litter, and root samples were oven-killed at 105 °C for 30 min to halt enzymatic activity and then oven-dried at 65 °C for approximately 72 h until a constant weight was achieved (Yu et al. 2010). All dried biomass and air-dried soil samples were ground into a fine powder using a ball mill and passed through a 0.15-mm sieve. Carbon (C), hydrogen (H), oxygen (O), and nitrogen (N) contents were then

determined at the functional group level using an elemental analyser (FlashSmart, Elementar, Germany). Based on these measurements, elemental ratios (C:H:O:N, C:H:O, C:N, and C:O) were calculated for plant, litter, soil, and root samples (Peng et al. 2023).

Identification of ecosystem stability drivers

While traditional studies on ecosystem stability have focused on soil biodiversity, proposing that higher biodiversity confers greater ecosystem stability (Berdugo et al. 2020; Fu et al. 2025; Han et al. 2025; Qi et al. 2026), we here adopt a stoichiometry-based perspective. Ecosystem stability is defined as time-averaged plant productivity divided by its standard deviation (Yang et al. 2018). Drawing on this definition, we decomposed its four plant-litter-soil-root characterized dimensions: temporal scales, various properties, organizational structures and multiple thresholds (see the section "Computation of homeostatic regulation thresholds" for detailed descriptions). We further identified ecosystem regulatory sensitive indicators under the multi-threshold framework (i.e. Root-C and Root-H, Fig. 3d) and explored the factors that govern these indicators, which serve as the drivers of ecosystem stability. This hierarchical organization establishes multiple buffering thresholds that enable the ecosystem to resist perturbations driven by seasonality and cold-warm alternations and to avoid transitions to alternative stable states.

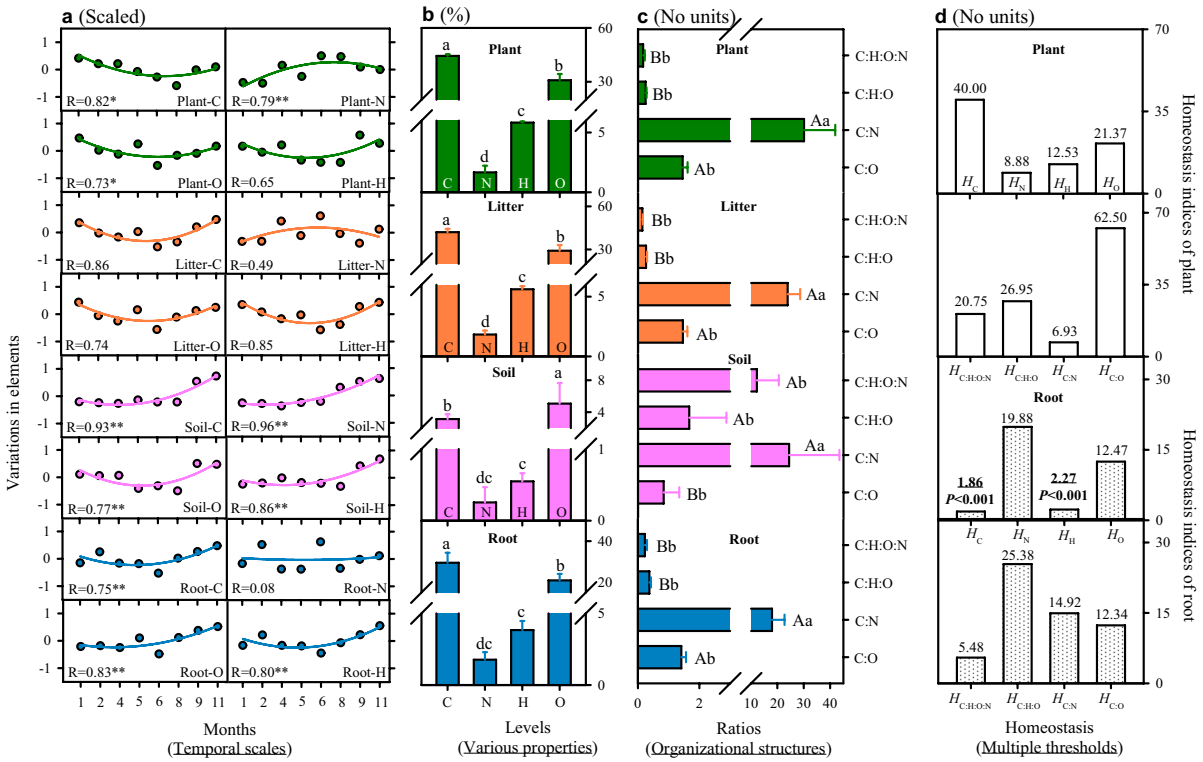


Fig. 3 Patterns of the ecosystem stability based on ecological stoichiometry from carbon (C), hydrogen (H), oxygen (O) and nitrogen (N) elements. Temporal scales are characterized by cooling and warming environments include January, February, April, May, June, August, September and November (**a**); various properties are reflected by plant, litter, soil and root (**b**); organizational structures are described by the ratios of C:H:O:N, C:H:O, C:N and C:O (**c**); multiple thresholds are expressed by the stoichiometric homoeostasis indices of plant and root (**d**). Values (mean ± SD) with the same uppercase letters (comparison between groups) and the lowercase letters (comparison within groups) are not significantly different at $P < 0.05$. * and ** significant correlation between the ecosystem elements and the months at the 0.05 and 0.01 level, respectively. Plant (Litter, Soil or Root)-C, -N, -O and -H: plant carbon, nitrogen, oxygen and hydrogen content, respectively

Computation of homeostatic regulation thresholds

The estimation of the homoeostatic regulation ability of every plant and root factors was carried out by means of calculating the homoeostatic regulation coefficient (H) based on the equation presented hereinafter (Sterner and Elser 2002):

$$y = cx^{1/H}$$

where y is the C, N, H or O content (% dry mass) or C:H:O:N, C:H:O, C:N or C:O ratio of plant (or root), x is the C, N, H or O content or C:H:O:N, C:H:O, C:N or C:O ratio in the soil and $c$represents a constant (Yu et al. 2010).

When the result of linear regression analysis is not significant ($P > 0.05$), y is in an absolute steady state. When the result is significant ($P < 0.05$), plants (or roots) are classified into four types: if $H > 4$, it indicates that y is in a homeostatic; if $2 < H < 4$, it means that y is in a weakly homeostatic; if $4/3 < H < 2$, it shows that y is in a weakly plastic; if $H < 4/3$, it implies that $y$is in a plastic (Persson et al. 2010).

From field in-situ observations to global drylands

Insights derived from long-term *in-situ*observations are critical for identifying key mechanisms and indicators that underpin ecosystem stability and functioning. Such field-based evidence helps capture realistic environmental constraints, biotic interactions, and dynamic feedbacks that cannot be fully represented by controlled experiments or remote sensing products alone. Once robust mechanisms and diagnostic indicators are identified at the local scale, scaling these findings to global dryland regions becomes increasingly meaningful for both theoretical advancement and practical application. Global drylands are highly vulnerable to climate warming, drought intensification, and seasonal fluctuations, yet their responses remain underrepresented in large-scale models. Extrapolating locally validated mechanisms to the global dryland extent can improve the accuracy of model projections, reveal consistent response patterns across heterogeneous regions, and support the development of early-warning indicators for ecosystem degradation. Therefore, transitioning from site-specific mechanistic discovery to large-scale prediction represents an essential step toward a more comprehensive and predictive understanding of dryland ecosystem stability under global change (Kanniah et al. 2009; Yao et al. 2020). Following the methods previously described by (Ge et al. 2018), mechanistic investigations of targeted scientific questions and the identification of key factors are carried out at an*in-situ* plot scale, and the corresponding findings are extrapolated to global scales to perform model simulations and predictions. In this work, at the *in-situ* plot scale, we identified the primary explanatory variables shaping ecosystem sensitivity indicators through field surveys and laboratory analyses. At the global scale, using CMIP6 outputs, we projected the evolving trajectories of these indicators, revealing that elevated core driving variable levels are required to regulate such indicators under diverse future scenarios.

Statistical analysis and future projections

To make a systematic and effective study on the drivers of ecosystem stability, we first performed 'max–min' normalization on the data based on *in-situ* observations, where it was calculated as [actual value (α_i)-mean value ($\bar{\alpha}$)]/[maximum (α)-minimum (α)]. Consistent with previous research (Chen et al. 2019), then we applied three statistical methods—partial correlation study, variation partitioning assessment and structural equation modelling analysis—to check whether the importance of Root-O remained consistent when accounting for the other three kinds of factors.

Given the significant interlinkages and interdependencies among multiple factors, partial correlation analysis was first performed to quantify the relationships between ecosystem sensitivity indicators driving threshold variations (i.e. Root-C and Root-H) and various influencing factors. Specifically, partial correlation analyses were conducted to examine the association between [Variable A] and [Variable B], with [Variable C] statistically controlled for. The significance level was set at $\alpha = 0.05$ for two-tailed tests, and we reported the partial correlation coefficient (r_p) along with the corresponding P-value. For instance, after individually controlling for each individual variable related to root property, we investigated the relationships between Root-C/Root-H and the properties of plant, litter and soil. A greater deviation in the partial correlation coefficient between the zero-order

correlation (uncontrolled) and the controlled correlation indicates a stronger influence of the regulated factor (Doetterl et al. 2015). Furthermore, a larger magnitude of this deviation also denotes more robust interaction effects among these predictor variables (Chen et al. 2019). All aforementioned analyses were implemented using SPSS 27.0 (SPSS, Inc., Chicago, IL, USA) and Edraw Mind Map 7.9 was utilized for supplementary visualization purposes.

Variation partitioning assessment was conducted to disentangle the individual and joint contributions of different factor groups (e.g. plant traits, soil properties) to the variance in ecosystem sensitivity indicators driving threshold variations (Chen et al. 2019). All analyses were implemented in*R* v4.3.3 using the *vegan* package (v.3.6.1), with key methodological details specified to ensure reproducibility as follows: (1) Core analytical function. We employed the 'varpart ()' function—the dedicated tool for variation partitioning in *vegan*—rather than 'adonis ()' (PERMANOVA). This choice was justified by the fact that 'varpart ()' is optimized for decomposing variance in univariate response variables (i.e., Root-C and Root-H) into unique and shared components across multiple predictor groups (Legendre 2007). In contrast, 'adonis ()' is designed for permutational multivariate analysis of variance based on distance matrices, which is incompatible with our univariate analytical framework. (2) Parameter settings. (i) Permutation tests: A total of 999 permutations were implemented (default = 99) to assess the statistical significance of variance components. This setting is a well-recognized practice in ecological research to enhance the robustness of inference for contribution rates. (ii) Sum of squares (SS): Type I (sequential) SS was applied, consistent with the default configuration of 'varpart ()'. This approach sequentially quantifies the variance explained by each predictor in the order of input, aligning with the standard protocol for linear model-based variation partitioning. (3) Data processing. Negative values of explained variance (R^2) for any predictor group were set to zero, as such values indicate that the predictor group explains less variation than randomly generated normal variables (Delgado-Baquerizo et al. 2017). (4) Output reporting. We reported the unique contribution (accompanied by R^2 values and permutation *P*-values), shared (joint) contribution, and total explained variance for each predictor group.

Structural equation modelling (SEM) was used further to check the direct and indirect links between Root-C/Root-H and plant, litter root and soil properties. This methodology can divide the direct and indirect impacts that a single variable can have on another, and it is consequently beneficial for probing into the intricate relationships in natural ecosystems. Given the strong intercorrelations among factors within each group, we first performed principal component analysis (PCA) to construct a multivariate functional index before developing the SEM. This index is a comprehensive value derived by integrating multiple correlated indicators that represent the same ecological function. The first component (PC1), identified by the key variables from each respective group (i.e., Plant-CHON, Litter-C, Soil-N, and Root-O), served as the cornerstone for subsequently analyses, representing the integrated properties of the system. An a priori SEM was subsequently formulated to elucidate the causal mechanisms—both direct and indirect—linking plant, litter, soil and root attributes to Root-C and Root-H, which serve as sensitive proxies for ecosystem stability. SEM accommodates categorical exogenous variables, as these variables are exempt from the model's distributional assumptions (Grace 2006). Path coefficients were estimated using maximum likelihood, following natural log-transformation of the standard deviation to maximize linearity with predictors (Shi et al. 2016). We picked a final SEM by considering the overall goodness-of-fit (Eldridge et al. 2018), including chi-square (χ^2)/degree of freedom (df), root mean square residual (RMR), and comparative fit index (CFI). The hypothesized model is deemed to fit the data well if the χ^2/df ratio and RMR approach 0, and the CFI approaches 1; otherwise, the model is rejected (Chen et al. 2019; Li et al. 2020). The structural equation modeling analyses were carried out by means of the AMOS 27.0 software (Amos Development Corporation, Chicago, IL, USA).

To project future changes in core sensitivity metrics under different climate change scenarios, we estimated trends in Root-C across global drylands through the end of the twenty-first century. We use Root-C as a representative here, given that the impact pathways of Root-C and Root-H are extremely similar, see Figs. 4, 5, and 6. The analysis was conducted under the corresponding Shared Socioeconomic Pathways (SSPs)—specifically the moderate-emission scenario (SSP2-4.5, an intermediate reference

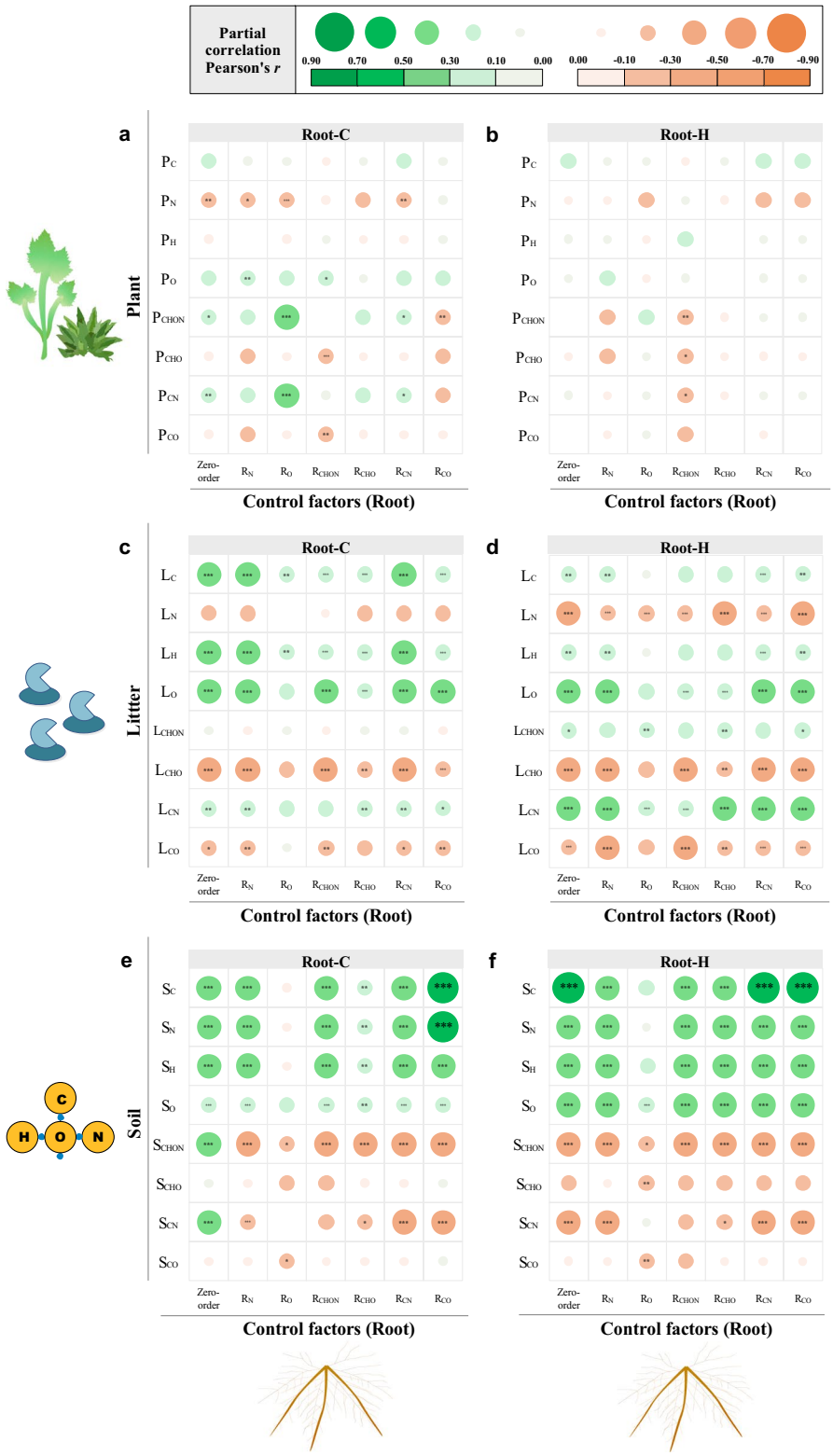


Fig. 4 Partial correlations between the Root-C/Root-H and the plant, litter and soil properties after controlling Root-O. The *x*-axis presents the zero-order (without any factors being controlled) and the controlled factors. The *y*-axis presents the factors (**a-b** plant, **c-d** litter, **e–f** soil properties) of which the correlations with the ecosystem stability are examined. The size and hues of the circles denote the intensity and sign of the correlation. P_C, Plant-C; P_N, Plant-N; P_H, Plant-H; P_O, Plant-O; P_{CHON}, Plant-C:H:O:N; P_{CHO}, Plant-C:H:O, P_{CN}, Plant-C:N; P_{CO}, Plant-C:O. Similarly, "L", "S", "R" is litter, soil and root, respectively. $^{*}0.05 < P < 0.1$; $^{**}P < 0.05$; $^{***}P < 0.01$

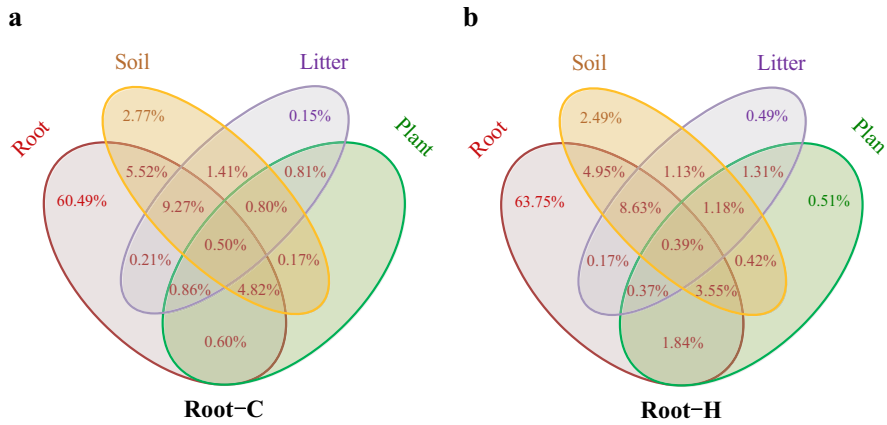


Fig. 5 Relative contributions of root, soil, litter and plant properties to the Root-C/Root-H. Variation partitioning assessment was carried out to determine the variance in the Root-C (**a**) and Root-H (**b**) explained by these four groups of root, soil, litter and plant factors

scenario for future climate change) and high-emission scenario (SSP5-8.5, representing the most extreme pathway with the greatest warming magnitude) over the 1950–2100 period—using outputs from the latest Coupled Model Intercomparison Project Phase 6 (CMIP6, (Gidden et al. 2019). All raw model outputs were retrieved, downloaded and validated via the official CMIP6 archive (https://pcmdi.llnl.gov/CMIP6/), following the unified data format, variable naming conventions and experimental protocols of CMIP6. The ensemble means of selected CMIP6 models, including EC-Earth3-CC, IPSL-CM6A-LR, NorESM2-LM, and NorESM2-MM, account for uncertainties in inter-model variability and yield more robust predictions than any single model. Their land surface modules include carbon allocation schemes for aboveground and belowground vegetation biomass and can generate gridded Root-C estimates. A multi-model ensemble was constructed using the arithmetic mean, and individual model outputs were retained to quantify inter-model uncertainty and compare differences in Root-C allocation and accumulation simulated by distinct land surface modules. Given that the historical results from CMIP6 end in 2014, we extend them to 2100 by integrating them with the SSP2-4.5 and SSP5-8.5 scenarios.

Results

Traditional characteristics of ecosystem stability

Across global dryland ecosystems, our spatiotemporal trend analysis reveals that regional warming patterns are closely associated with shifts in dryland distribution. Specifically, temperature-induced changes in the aridity index (i.e. the ratio of annual precipitation to potential evapotranspiration) have reshaped dryland distribution patterns, as supported by the observed spatial heterogeneity in Figs. 2a, b. The aridity index gradually increases from extremely arid regions to sub-humid areas, and this pattern corresponds well with variations in the leaf area index and soil biodiversity index (Figs. 2c, d). With rising soil organic carbon and soil water content (Figs. 2e, f), these variables modulate soil quality via physiochemical and biological processes, which further determine the functional distribution of plants and soil biota. These findings demonstrate that rising temperatures have altered dryland extent, reduced vegetation cover, and diminished soil biodiversity, ultimately weakening ecosystem stability. The sustainability of carbon and water cycles provides essential resources that underpin soil biodiversity, thereby consolidating the stability and functional resilience of dryland ecosystems.

Key drivers of ecosystem stability

Carbon (C), hydrogen (H), oxygen (O) and nitrogen (N) exhibited distinct seasonal trends in the properties of plant, soil, litter and root across environments moving from cooling to warming (Fig. 3a). The C contents in plant, litter and root properties were significantly higher than their N, H and O contents (all $P < 0.05$). However, for soil, O contents was greater than that of the other elements ($P < 0.05$) (Fig. 3b). The C:N ratio was distinctly larger than the C:H:O:N, C:H:O and C:O ratios in plant, litter, soil and root,

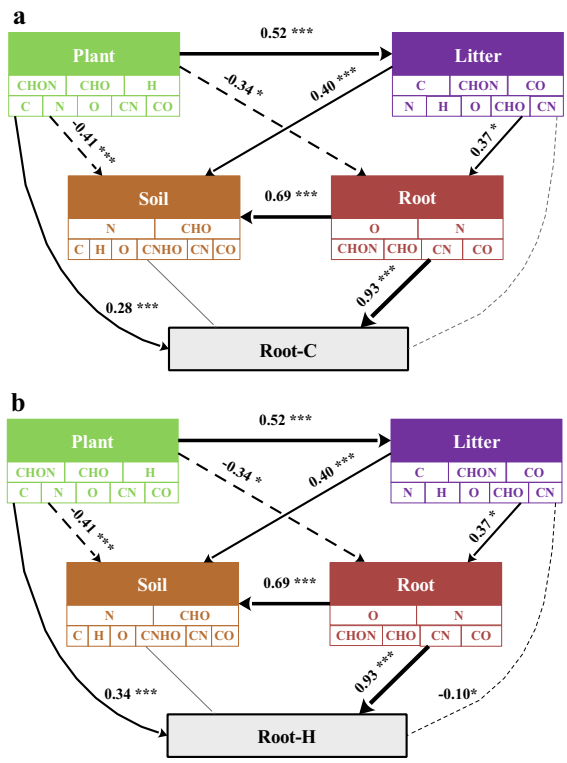


Fig. 6 Direct and indirect effects of plant, litter, soil and root properties on the Root-C/Root-H. The structural equation modelling was carried out for two variants, namely Root-C (**a**) and Root-H (**b**). Black solid arrows signify positive relationships, while black dotted arrows denote negative relationships. Grey arrows represent insignificant relationships. The width of the arrow is commensurate with the intensity of the relationship. Multiple-layer rectangles symbolize the first component from the Principal Component Analysis performed on the properties of plant, litter, soil and root. The results of the optimal model fitting: chi-square ($\chi.^2$)/degree of freedom (df) < 0.001, root mean square residual (RMR) < 0.001, comparative fit index (CFI) > 0.95, akaike information criterion (AIC) = 30.00. *0.05 < P < 0.1; **P < 0.05; ***P < 0.01

respectively (all $P < 0.05$). Furthermore, the C:H:O:N and C:H:O ratios in soil were considerably higher than those in plant, litter and root ($P < 0.05$) (Fig. 3c). The values of H fluctuated within the ranged of 1.86 to 62.5 across all factors. Therein, the H values of C and H were 1.86 and 2.27 correspondingly (all $P < 0.001$) in root, and these values (i.e., Root-C and Root-H) were obviously lower than the homeostatic value (Fig. 3d).

Partial correlation analysis revealed that, without controlling for Root-O (zero-order in Fig. 4), ecosystem sensitivity indicators driving threshold variations—represented by Root-C and Root-H—were correlated, either weakly or strongly, with plant, litter and soil properties. However, after controlling for Root-O, the correlation coefficients between Root-C/Root-H and plant, litter, soil properties changed by approximately + 36%, − 50% and − 58%, respectively (Fig. 4). Variation partitioning assessment further demonstrated that mainly Root-O accounted for a substantially larger proportion of the variance (63.75%) in Root-H compared to soil (2.49%), litter (0.49%) and plant (0.51%) (Fig. 5b). Similarly, the preponderant contribution of Root-O was also noted in the case of the Root-C (Fig. 5a). Structural equation modelling (SEM) analysis also disclosed that Root-O had the largest direct effect (all standardized path coefficients equal 0.93) that regulated the Root-C and Root-H (Fig. 6a, b). Taken together, the three statistical methods revealed that Root-O acts as a crucial factor in modulating ecosystem sensitivity indicators driving threshold variations.

Future projections of the ecosystem sensitivity indicator

Our study further presents future projections of Root-C storage across global drylands—a critical biogeochemical indicator closely linked to ecosystem functional stability, resilience, and belowground C sequestration capacity (Fig. 8). Based on the multi-model mean derived from four CMIP6 models, we project substantial increases in the anomaly of Root-C content across global drylands by the end of the twenty-first century relative to the 1950–2014 historical baseline. Specifically, Root-C storage is anticipated to rise by approximately 30 g C m^{-2} under the moderate-emission SSP2-4.5 scenario and by nearly 60 g C m^{-2} under the high-emission SSP5-8.5 scenario by 2100 (Fig. 8a). Temporal dynamics from 1980 to 2100 further reveal that the annual Root-C anomaly remains consistently higher under SSP5-8.5 than under SSP2-4.5 throughout the entire projection period (Figs. 8b, c). This pronounced divergence underscores that future anthropogenic forcing—particularly under unmitigated high-emission pathways—exerts a dominant and amplifying control over long-term Root-C dynamics in dryland ecosystems. Collectively, these projections imply that future increases in Root-C across global drylands will likely be sustained and potentially intensified by an

enhanced Root-O under ongoing anthropogenic climate warming, as supported by mechanistic relationships illustrated in Fig. 7. Such climate-driven increments in belowground C storage may partially offset atmospheric C enrichment while modifying resource allocation, nutrient cycling, and carbon–water coupling in water-limited ecosystems. However, the magnitude and persistence of these trends remain contingent upon interactive effects between rising temperatures, shifting precipitation regimes, and adaptive responses of root physiological functioning, highlighting the need for continued model refinement and long-term observational constraints to reduce projection uncertainty.

Discussion

Climate warming has triggered cascading ecological perturbations across dryland ecosystems, driving shifts in dryland distribution, reductions in vegetation cover, declines in soil biodiversity, and ultimately imposing severe constraints on ecosystem stability. Our findings (Fig. 2) are broadly consistent with the classical conceptual framework of sequential ecosystem degradation, as documented in previous research (Berdugo et al. 2020; Fu et al. 2025; Han et al. 2021; Huang et al. 2020a). Collectively, these works delineate four interconnected phases of stability loss: gradual climate warming, subsequent vegetation alteration, severe soil degradation, and eventual ecosystem collapse. Under the IPCC high-emission scenario (RCP 8.5), projected climatic warming is expected to drive an approximately 51.6% decline in species richness by 2100. Such impacts will be disproportionately concentrated in ecologically insecure regions, thereby exacerbating risks to the structural and functional integrity of dryland ecosystems (Fu et al. 2025).

Ecologically insecure regions were delineated using an ecological security index (ESI) with a critical threshold of ESI ≥ 1.1, which is mathematically defined as $\mathrm{ESI} = \sqrt[3]{(\mathrm{OC}/\mathrm{OP}) \times \mathrm{Twm} \times (\mathrm{PET}/\mathrm{P})} \times C_{\mathrm{constant}}$. This index integrates five fundamental biophysical and climatic variables: oxygen production (OP), oxygen

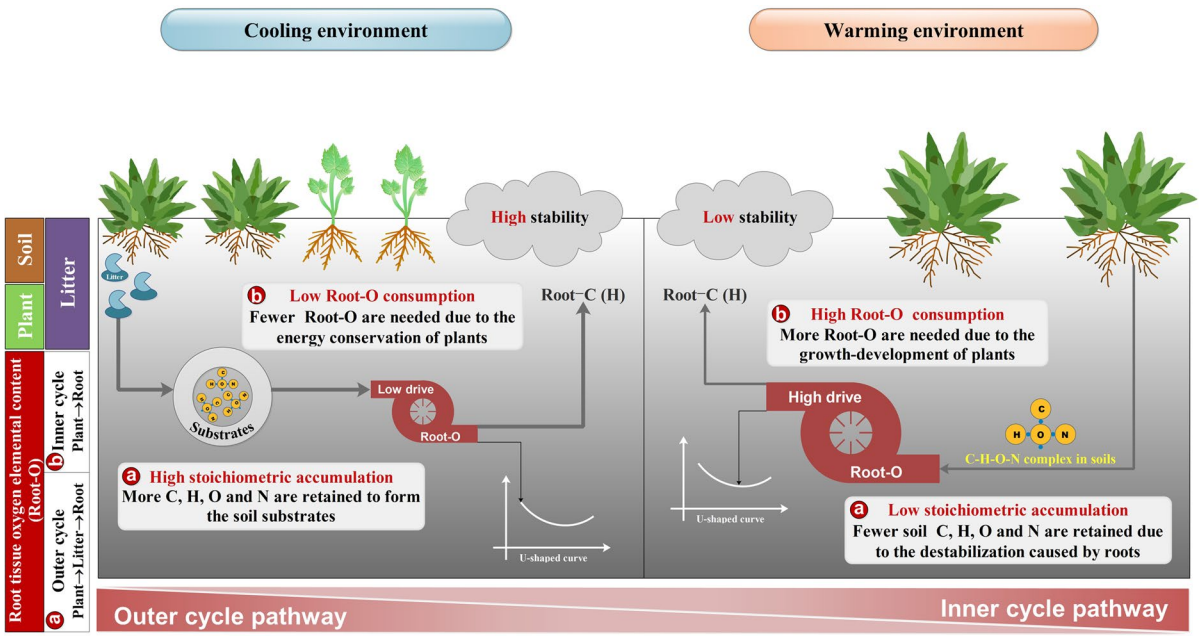


Fig. 7 Schematic framework of dryland ecosystem stability and its driving factors. From cooling environment to warming environment, more Root-O are needed due to the growth-development of plants, fewer soil C, H, O and N are retained owing to the destabilization caused by roots (**a-b**). Pathways which delineate the outer cycle commencing from plant, transitioning to litter, and subsequently leading to root. Meanwhile, the pathway has been established to define the inner cycle from the plant to the root. Notably, this mechanism framework is constructed based on multi-dimensional analytical approaches, among which structural equation modelling serves as one representative method to disentangle direct and indirect factors

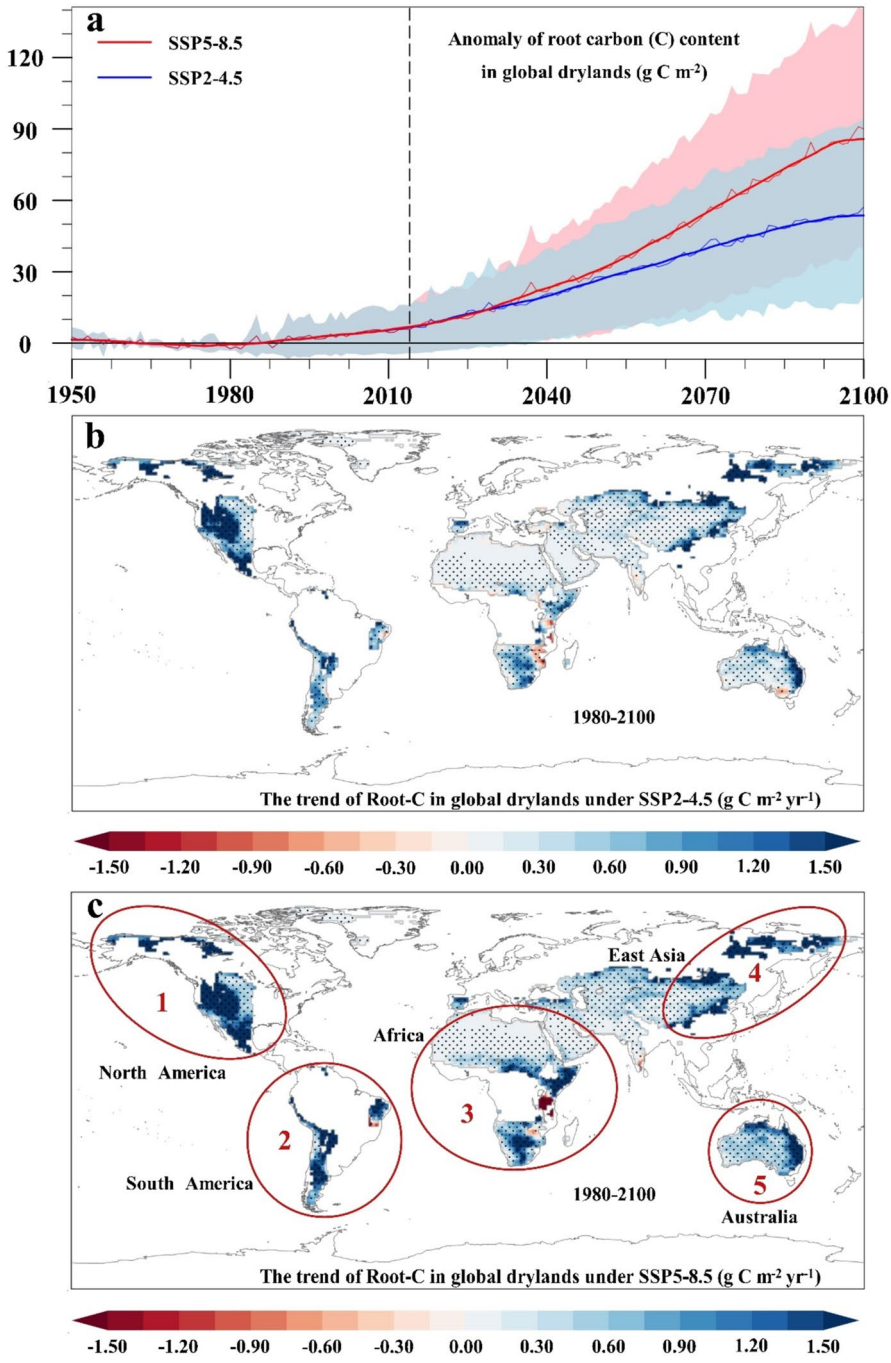


Fig. 8 Temporal and spatial variation in the global mean Root-C of drylands. The temporal anomaly of Root-C is shown in (**a**), and the spatial trends of Root-C under SSP2-4.5 and SSP5-8.5 are shown in (**b**)and (**c**), respectively. The shading and stippling denote the 95% confidence intervals. Based on the carbon-oxygen coupling relationship and the findings of this study, the regions highlighted by red circles in drylands may indicate a relatively stronger Root-O under future conditions; the regional delineation is adapted from (Yao et al. 2020)

consumption (OC), temperature warming magnification (Twm), precipitation (P), and potential evapotranspiration (PET), following the well-established framework proposed by (Huang et al. 2020a). Importantly, the ESI framework quantifies ecosystem security by explicitly anchoring its assessments in the dynamic oxygen cycle between terrestrial ecosystems and the overlying atmosphere, thereby providing a robust mechanistic foundation for evaluating ecological stability under ongoing climate change (Fu et al. 2025; Huang et al. 2020a). By centering on oxygen dynamics—a core functional indicator of ecosystem metabolism—this approach

enables reliable identification of vulnerable regions and strengthens mechanistic interpretations of how climate warming drives progressive ecosystem degradation and functional collapse in drylands.

Through a suite of complementary analytical and statistical methods, our findings advance current understanding by identifying with empirical support—that Root-O exhibits significantly stronger predictive power than other covariates in explaining key ecosystem sensitivity indicators driving threshold variations, as illustrated in Figs. 3, 4, 5, and 6. During the environmental transition from cooling to warming regimes, the dynamics of elemental contents of numerous attribute-related indicators exhibit a U-shaped curve, with low values in the warm season and high values in the cold season (Fig. 3a). According to kinetic theory, the constraints on decomposition and partitioning imposed by biotic and chemical processes are strongly modulated by temperature (Davidson and Janssens 2006; Zhang et al. 2025). Therefore, we constructed a conceptual framework of ecosystem stability, namely the elemental contents of dryland ecosystem indicators increased alongside both the relative contribution of the outer cycling pathway (mediated by plant-litter-root linkages) and soil stoichiometric ratios (C, H, O, and N) for elemental accumulation. Conversely, the elemental contents of ecosystem indicators declined with intensification of Root-O consumption driven by the inner cycling pathway (plant-root linkages), as depicted in Fig.7. This conceptual framework highlights the central role of Root-O dynamics in modulating dryland ecosystem stability under climate transitions, offering new mechanistic insights into the differential regulatory roles of internal and external biogeochemical cycles.

The decline in elemental contents of dryland ecosystem indicators is associated with the enhanced Root-O consumption by inner cycle pathway. In warm environmental contexts, Root-O consumption rises markedly (Fig. 3a). Key processes including C mineralization and C distribution govern root growth. For instance, accelerated root respiration linked to temperature sensitivity-Q_{10}(Davidson and Janssens 2006), regulates taproot elongation, abundant lateral root formation and root hair development (Armstrong et al. 2009; Warren et al. 2015). Meanwhile, to better absorb nutrients such as N, taproots extend deep into the soil, lateral roots spread widely like branches and root hair numbers increase significantly (Norby and Jackson 2000; Ridgeway et al. 2024). These processes require substantial metabolic energy, which is primarily supplied through aerobic respiration, thereby increasing root oxygen demand (Armstrong et al. 2009; Norby and Jackson 2000). Consistent with this deduction, when plant roots are unable to obtain enough oxygen to carry out aerobic respiration, the production of energy will be restricted and the ability of roots to absorb nutrients will decline (Norby and Jackson 2000; Warren et al. 2015), which may lead to essential changes in Root-O, further altering its effect values on Root-C and Root-H and easily breaking the stability of local ecosystems.

Plants do not exist in isolation. They constitute the primary source of litter in terrestrial ecosystems, and litter decomposition acts as a fundamental pathway modulating nutrient availability for root growth, which in turn mediates plant performance, forming a nutrient cycle. Enough nutrient release from decomposing litter effectively sustains root growth and physiological activity, whereas limited nutrient supply constrains root metabolic performance and biomass accumulation (Ridgeway et al. 2024). This regulatory effect is particularly pronounced in resource-poor desert ecosystems, where sparse litter production and low decomposition rates induce persistent nutrient limitation, resulting in retarded root growth and adaptive morphological shifts such as increased root elongation and reduced diameter to enhance soil foraging efficiency (Huang et al. 2021; Yang et al. 2023). Conversely, under favorable rhizosphere conditions, root exudates rich in labile sugars and amino acids provide readily available energy for soil microorganisms, thereby stimulating microbial decomposition of soil organic matter (SOM). Typically, SOM consists of 45–58% C, 3–6% H, 30–40% O, and 2–5% N, whose mineralization dynamically modifies soil elemental stoichiometry, further shaping rhizosphere nutrient cycling and root-soil feedbacks (Angst et al. 2021).

This study further extrapolates field observations obtained at a semi-arid grassland site to global dryland ecosystems, yet this scaling approach carries inherent constraints. These constraints mainly come from the fact that we used only one experimental site, which can only show the common biogeochemical features of semi-arid grasslands. Global drylands span extremely-arid, arid, semi-arid and sub-humid subtypes with divergent soil substrates

and plant assemblages (Huang et al. 2016, 2017); our dataset cannot fully encompass this broad environmental spectrum, which introduces quantitative uncertainties when generalizing site-scale patterns to the worldwide dryland biome. Importantly, such limitations only affect the magnitude of biogeochemical responses across regions, rather than ignoring the core driving mechanisms of ecosystem stability mediated by Root-O uncovered in this work. As demonstrated by this cross-scale analysis (Ge et al. 2018), it effectively connects fine plot-level mechanistic processes to broad macroecological patterns and provides tentative yet fundamental insights into global dryland biogeochemical cycling. Based on the above identified driving mechanism, regions including North America, South America, Africa, East Asia, and Australia will demand an elevated supply of Root-O under projected climate warming to maintain the stability and functioning of dryland ecosystems (Fig.8). Future coordinated multi-site field investigations across diverse dryland subtypes will supplement missing environmental gradients and further refine the quantitative generalizability of our conclusions.

Conclusions

We highlight that this study provides a well-defined framework for exploring how Root-O responds to plant, root, litter, and soil-related factors in the context of dryland ecosystem stability. The introduced framework can be used to distinguish warm and cold thermal regimes regulating Root-O content, which further reveals the ecological consequences of ecosystem shifts, especially within sensitive and fragile biomes. A key challenge is to validate the "FeiTian" Ecological Security Grand Model based on Root-O content via systematic measurements, thereby enabling accurate prediction of ecosystem sensitivity indicators that drive threshold variations under a changing environment. Overall, expansion of the existing network for Root-O measurements is a top priority.

Acknowledgements This work was jointly supported by Fundamental and Interdisciplinary Disciplines Breakthrough Plan of the Ministry of Education of China (JYB2025XDXM910) and the '111 Center' (B25040).

Data availability All the data employed in this study can be obtained gratis from the corresponding author upon submission of a reasonable request.

Declarations

Conflict of interest The authors declare no conflict of interest.

Open Access This article is licensed under a Creative Commons Attribution-NonCommercial-NoDerivatives 4.0 International License, which permits any non-commercial use, sharing, distribution and reproduction in any medium or format, as long as you give appropriate credit to the original author(s) and the source, provide a link to the Creative Commons licence, and indicate if you modified the licensed material. You do not have permission under this licence to share adapted material derived from this article or parts of it. The images or other third party material in this article are included in the article's Creative Commons licence, unless indicated otherwise in a credit line to the material. If material is not included in the article's Creative Commons licence and your intended use is not permitted by statutory regulation or exceeds the permitted use, you will need to obtain permission directly from the copyright holder. To view a copy of this licence, visit http://creativecommons.org/licenses/by-nc-nd/4.0/.

References

Angst G, Mueller KE, Nierop KGJ, Simpson MJ (2021) Plant- or microbial-derived? A review on the molecular composition of stabilized soil organic matter. Soil Biol Biochem 156:108189

Armstrong W, Webb T, Darwent M, Beckett PM (2009) Measuring and interpreting respiratory critical oxygen pressures in roots. Ann Bot 103:281–293

Ascha M, Bhattacharyya A, Ramos JA, Tonelli AR (2018) Pulse oximetry and arterial oxygen saturation during cardiopulmonary exercise testing. Med Sci Sports Exerc 10:1992–1997

Berdugo M, Delgado-Baquerizo M, Soliveres S, Hernández-Clemente R, Zhao Y, Gaitán J et al (2020) Global ecosystem thresholds driven by aridity. Science 367:787–790

Calvin M (1956) The photosynthetic carbon cycle. J Chem Soc, pp 1895–1915

Chameides WL, Perdue EM (1997) Biogeochemical cycles: a computer-interactive study of Earth system science and global change. Oxford University Press

Chen L, Liu L, Qin S, Yang G, Fang K, Zhu B, Kuzyakov Y, Chen P, Xu Y, Yang Y (2019) Regulation of priming effect by soil organic matter stability over a broad geographic scale. Nat Commun 10:5112

Davidson EA, Janssens IA (2006) Temperature sensitivity of soil carbon decomposition and feedbacks to climate change. Nature 440:165–173

Delgado-Baquerizo M, Eldridge DJ, Maestre FT, Karunaratne SB, Trivedi P, Reich PB, Singh BK (2017) Climate legacies drive global soil carbon stocks in terrestrial ecosystems. Sci Adv 3:e1602008

Doetterl S, Stevens A, Johan S, Merckx R, Oost KV, Pinto MC et al (2015) Soil carbon storage controlled by interactions between geochemistry and climate. Nat Geosci 8:780–783

Eldridge D, Maestre F, Koen T, Delgado-Baquerizo M (2018) Australian dryland soils are acidic and nutrient-depleted, and have unique microbial communities compared with other drylands. J Biogeogr 45:2803–2814

Fu L, Huang J, Zhang G, Han D, Ding L, Wei Y, Liu X, Li C, Yu H (2025) Abrupt loss of species richness caused by ecosystem transition. Sci Bull 70:1523–1532

Ge J, Zheng C, Xie H, Xin Y, Huang J, Fu Q (2018) Mid-latitude cirrus clouds at the SACOL site: macrophysical properties and large-scale atmospheric states. J Geophys Res Atmos 123:2256–2271

Gidden M, Riahi K, Smith S, Fujimori S, Luderer G, Kriegler E et al (2019) Global emissions pathways under different socioeconomic scenarios for use in CMIP6: a dataset of harmonized emissions trajectories through the end of the century. Geosci Model Dev 12:1443–1475

Grace JB (2006) Structural equation modeling and natural systems. Cambridge University Press

Greabu M, Battino M, Mohora M, Olinescu R, Totan A, Didilescu A (2008) Oxygen, A paradoxical element? Rom J Intern Med 2:125–135

Grünzweig J, De Boeck H, Rey A, Santos M, Adam O, Bahn M et al (2022) Dryland mechanisms could widely control ecosystem functioning in a drier and warmer world. Nat Ecol Evol 6:1064–1076

Guan X, Huang J (2024) Constructing semi-arid ecological barriers to prevent desertification. Innov Geosci 2:100067

Han D, Huang J, Ding L, Liu X, Li C, Yang F (2021) Oxygen footprint: an indicator of the anthropogenic ecosystem changes. Catena 206:105501

Han D, Huang J, Ding L, Zhang G, Liu X, Li C, Yang F (2022) Breaking the ecosystem balance over the Tibetan Plateau. Earth's Future 10:e2022EF002890

Han D, Huang J, Liu X, Fu L, Ding L, Zhang G, Li C, Yang F, Shi J, Zhang B (2025) Silent soils have been awakened by climate change. CATENA 252:108777

Huang J, Guan X, Ji F (2012) Enhanced cold-season warming in semi-arid regions. Atmos Chem Phys 12:5391–5398

Huang J, Yu H, Guan X, Wang G, Guo R (2016) Accelerated dryland degradation under climate change. Nat Clim Change 6:166–172

Huang J, Yu H, Dai A, Wei Y, Kang L (2017) Drylands face potential threat under 2℃ global warming target. Nat Clim Change 7:417–422

Huang J, Yu H, Han D, Zhang G, Wei Y, Huang J, An L, Liu X, Ren Y (2020a) Declines in global ecological security under climate change. Ecol Indic 117:106651

Huang J, Zhang G, Zhang Y, Guan X, Wei Y, Guo R (2020b) Global desertification vulnerability to climate change and human activities. Land Degrad Dev 31:1380–1391

Huang W, Wang K, Ye C, Hockaday WC, Wang G, Hall SJ (2021) High carbon losses from oxygen-limited soils challenge biogeochemical theory and model assumptions. Glob Change Biol 27:6166–6180

Hulme M (1996) Recent climatic change in the world's drylands. Geophys Res Lett 23:61–64

Jiang G, Men X, Fu Z, Zeng L, Hu W, Gao S et al (2026) Thaw slumps alter ecosystem carbon budget in alpine grassland on the Tibetan Plateau. Nat Commun 17:190

Kanniah KD, Beringer J, Hutley LB, Tapper NJ, Zhu X (2009) Evaluation of collections 4 and 5 of the MODIS gross primary productivity product and algorithm improvement at a tropical savanna site in northern Australia. Remote Sens Environ 113:1808–1822

Kuzyakov Y, Xu X (2013) Competition between roots and microorganisms for nitrogen: mechanisms and ecological relevance. New Phytol 198:656–669

Legendre P (2007) Studying beta diversity: ecological variation partitioning by multiple regression and canonical analysis. J Plant Ecol 1:3–8

Li X, Guo Y (2025) Paradigm shifts from data-intensive science to robot scientists. Sci Bull 70:14–18

Li J, Pei J, Pendall E, Fang C, Nie M (2020) Spatial heterogeneity of temperature sensitivity of soil respiration: a global analysis of field observations. Soil Biol Biochem 141:107675

Li C, Huang J, Ding L, Liu X, Han D, Huang J (2021) Estimation of oceanic and land carbon sinks based on the most recent oxygen budget. Earth's Future 9:e2021EF002124

Liu J, Shen S, Zhu K, Li Z, Chen N, Lichtfouse E, Jia H (2024) Novel insights into the factors influencing rhizosphere reactive oxygen species production and their role in polycyclic aromatic hydrocarbons transformation. Soil Biol Biochem 198:109562

Liu J, Wang H, Mou J, Penuelas J, Delgado-Baquerizo M, Martiny A et al (2025) Global-scale shifts in marine ecological stoichiometry over the past 50 years. Nat Geosci 18:769–778

Luo L, Sun T, Pan Z, Lv J, Peňuelas J, Sardans J et al (2025) Rethinking organic carbon sequestration in agricultural soils from the elemental stoichiometry perspective. Glob Change Biol 31:e70319

Maestre FT, Eldridge DJ, Gross N, Bagousse-Pinguet YL, Saiz H, Gozalo B, Ochoa V, Gaitán JJ (2022) The BIODESERT survey: assessing the impacts of grazing on the structure and functioning of global drylands. Web Ecol 22:75–96

Norby RJ, Jackson RB (2000) Root dynamics and global change: seeking an ecosystem perspective. New Phytol 147:3–12

Peng J, Ma F, Tian D, Quan Q, Chen C, Liao J, Zhou Q, Niu S (2023) Plant C:N ratio predicts community composition changes under N addition in an alpine meadow. J Ecol 111:589–600

Persson J, Fink P, Goto A, Hood JM, Jonas J, Kato S (2010) To be or not to be what you eat: regulation of stoichiometric homeostasis among autotrophs and heterotrophs. Oikos 119:741–751

Qi J, Liang C, Zhang C, Wang M, Wei G, Jiao S (2026) Intensifying aridity undermines the role of soil biodiversity in supporting ecosystem stability. Glob Chang Biol 32:e70903

Ridgeway J, Kane J, Morrissey E, Starcher H, Brzostek E (2024) Roots selectively decompose litter to mine nitrogen and build new soil carbon. Ecol Lett 27:e14331

Shi Z, Xu X, Souza L, Wilcox K, Jiang L, Liang J, Xia J, García-Palacios P, Luo Y (2016) Dual mechanisms regulate ecosystem stability under decade-long warming and hay harvest. Nat Commun 7:11973

Sterner RW, Elser JJ (2002) Ecological stoichiometry: the biology of elements from molecules to the biosphere. Princeton University Press

Toro G, Pinto M, Pimentel P (2018) Root respiratory components of *Prunus* spp. rootstocks under low oxygen: regulation of growth, maintenance, and ion uptake respiration. Sci Hortic 239:259–268

Wang G, Huang J, Guo W, Zuo J, Wang J, Bi J, Huang Z, Shi J (2010) Observation analysis of land-atmosphere interactions. J Geophys Res 115:DooK17

Warren JM, Hanson PJ, Iversen CM, Kumar J, Walker AP, Wullschleger SD (2015) Root structural and functional dynamics in terrestrial biosphere models-evaluation and recommendations. New Phytol 205:59–78

Yang G, Wagg C, Veresglou SD, Hempel S, Rillig MC (2018) How soil biota drive ecosystem stability. Trends Plant Sci 12:1057–1067

Yang F, Huang J, Zhou C, Yang X, Mamtimin A, Zheng X et al (2023) Desert abiotic carbon sequestration weakening by precipitation. Environ Sci Technol 57:7174–7184

Yao J, Liu H, Huang J, Gao Z, Wang G, Li D, Yu H, Chen X (2020) Accelerated dryland expansion regulates future variability in dryland gross primary production. Nat Commun 11:1665

Yu Q, Chen Q, Elser JJ, He N, Wu H, Zhang G, Wu J, Bai Y, Han X (2010) Linking stoichiometric homoeostasis with ecosystem structure, functioning and stability. Ecol Lett 13:1390–1399

Zhang G, He Y, Huang J, Fu L, Han D, Guan X, Zhang B (2023) Divergent sensitivity of vegetation to aridity between drylands and humid regions. Sci Total Environ 884:163910

Zhang X, Bi J, Zhu D, Meng Z (2024) Seasonal variation of net ecosystem carbon exchange and gross primary production over a Loss Plateau semi-arid grassland of northwest China. Sci Rep 14:2916

Zhang S, Zhao Y, Shi Y, Fang Q, Wang X, Fan J (2025) Global cooling drove diversification and warming caused extinction among Carboniferous-Permian fusuline foraminifera. Sci Adv 11:eadv2549

Zhu D, Bi J, Wang X, Meng Z, Shi J, Li O (2024) Diurnal asymmetry of surface albedo in a semi-arid grassland over the China's Loss Plateau. Atmos Sci Lett 25:e1271

Publisher's Note Springer Nature remains neutral with regard to jurisdictional claims in published maps and institutional affiliations.